10.21611/qirt.2023.08

Numerical and experimental analysis for flaw detection in composite structures of wind turbine blades using active infrared thermography

by A. A. A. Figueiredo*, G. D'Alessandro**, S. Perilli***, S. Sfarra**, H. Fernandes****

* *State University of Maranhao, Sao Luis, Brazil*
** *University of L'Aquila, L'Aquila, Italy*
*** *Sapienza University of Rome, Rome, Italy*
**** *Federal University of Uberlandia, Uberlandia, Brazil*

Abstract

Using composite materials in turbine blades has become common in the wind power industry due to their mechanical properties and low weight. This work aims to investigate the effectiveness of the active infrared thermography technique as a non-destructive inspection tool to identify defects in composite material structures of turbine blades. Experiments were carried out by heating the sample and capturing thermographic images using a thermal camera in four different scenarios, changing the heating strategy. Such a preliminary experiments are prodromic to build in the future the so-called optimal experiment design for thermal property estimation. Numerical simulations were carried out to present solutions for improving defect detection. It was demonstrated that active infrared thermography is an efficient technique for detecting flaws in composite material structures of turbine blades. This research contributes to advancing knowledge in inspecting composite materials.

1. Introduction

The blades of wind turbines are critical components and susceptible to various damages during their operation, which can affect other blades and turbines, increasing the costs of the energy generation process. The blades consist of two fiberglass composite halves held together by shear webs and strong adhesives. The composite structures of the blades can present different types of damage, such as delamination, cracks, air pockets, and fibre-matrix detachments. Adverse environmental conditions can also cause damage. The use of Non-Destructive Testing (NDT) to monitor the conditions of the blades is essential for the early detection of failures [1].

Infrared thermography is an NDT technique that detects internal defects in materials qualitatively and quantitatively without physical contact. The technique was developed to accurately predict the depth of defects and has successfully been applied in several areas. Infrared thermography offers a comprehensive approach to defect detection, allowing for large-area analysis and providing valuable information about the integrity of materials. Infrared thermography helps in decision-making for maintenance and quality control [2].

Different studies have used infrared thermography to detect faults in wind turbine blades. To the best of our knowledge, the first one can be attributed to A.P. Pontello, who in 1974 applied infrared thermography on turbine blades containing flaws covered by corrosion [3]. Passive infrared thermography was used to detect internal defects and evaluate the thermal behaviour of structures in different climatic conditions [4, 5]. Active thermography has been applied to qualitatively and quantitatively evaluate the presence of defects in turbine composite materials [6, 7].

The main objective of this work is to investigate the effectiveness of the active infrared thermography technique as a non-destructive inspection tool to identify defects in composite material structures of turbine blades. Experiments were conducted in the laboratory to detect an artificial polyvinyl chloride (PVC) inclusion in the sample. The active approach was applied by heating the sample through thermal resistances or a heating plate installed in transmission mode. The reproduced wind turbine blade cooled down naturally. A thermographic camera recorded thermal images of the sample's surface during the heating and cooling steps. Four different scenarios were analyzed to determine the best strategies for detecting the defect. Numerical simulations using the commercial software COMSOL® were carried out to study the experimental results and predict the numerical temperature distribution starting from the correct application of the boundary conditions. Since the defect is very thin, by considering the simmetry of the heating with respect to the size of the sample, the proposed thermal stimulus can be considered of interest to provide solid conclusions on the defect detection based on slight bendings of the thermal imprints [8].

2. Material and Methods

Figure 1 shows the configuration of the experiments performed, where the sample was characterized by two glass fibre/epoxy matrix composite plates and an artificial polyvinyl chloride (PVC) inclusion was considered a defect. Four different heating scenarios were designed to apply a thermal excitation to the sample. A FLIR T1020 thermal camera (1024 x 768 pixels resolution) was used to record thermal images from the front surface. Figure 1a shows an overview of the experiment, Fig 1b highlights the two heaters used on the rear surface, and Fig 1c shows the plate heater used in the last scenario.

Figure 2 presents in detail the sample used in the experiments, where each composite plate has a width, height and thickness equal to 203, 101, and 0.7655 mm, respectively. The PVC inclusion has a thickness of 0.17 mm and is located 0.30 mm away from the external surface (surface monitored by the thermal camera).

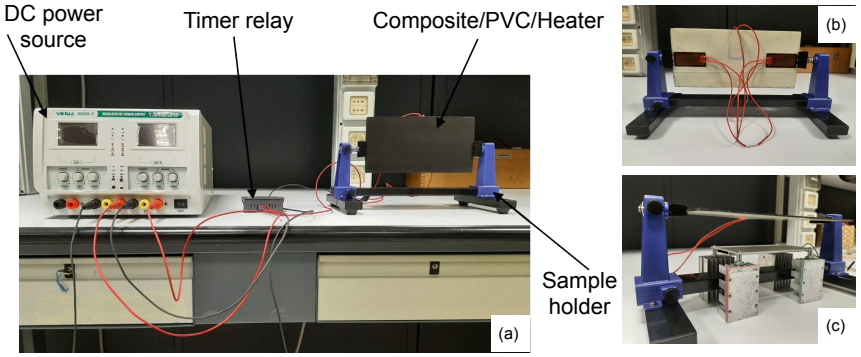

Fig. 1. *Experimental setup with IR camera in the laboratory: (a) overview, (b) two heaters, and (c) heater plate*

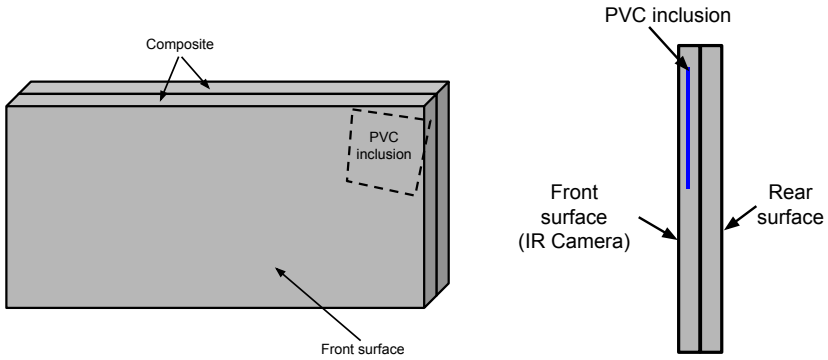

Fig. 2. *Geometry of the composite material and defect*

In scenario 1, a heater covered with polyimide layers of dimensions 44, 19, and 0.1 mm was inserted between the two composite plates and positioned as shown in Fig. 3a. Note that the particular symmetry of the heater-composite assembly built in scenario 1 not only allow the numerical modelling to be simplified, but also it represents the best practice for building the experimental apparatus used for thermal property estimation of solid materials when using the plane source method [9, 10]. In fact the analysis here reported can also be considered preliminary to the design of the experiment aimed at estimating the thermal properties of the composite material taking into account the presence of any inclusion. In scenario 2, two heaters with the same dimensions were inserted into the back surface and positioned as shown in Fig. 3b; it is observed that in this scenario there is a small region in common between the heater and the defect, but there is no contact between the two. Scenario 3 shown in Fig. 3c is the combination of scenarios 1 and 2, i.e., there is the central heater between the composites and two heaters on the rear surface. In scenario 4, a heat source of 400 W heating power with dimensions equal to 120, 70, and 2 mm was kept 37 mm away from the rear surface and positioned as in Fig. 3d. It is worth noting that in each scenario analyzed here, planar symmetry is applied to the heating to localize the inclusion without thermally stimulate all regions of the composite. This is a key point of the present work.

The heat transfer in the composite material and the PVC inclusion that occurs during experiments in different scenarios can be characterized by

$$k_i \nabla^2 T = \rho_i c_i \frac{\partial T}{\partial t} \tag{1}$$

where i represents the layers of the sample, composite (i=1), pvc (i=2). The k, c, and ρ are, respectively, thermal conductivity, specific heat, and density.

When the existing heat source between the composites is used, heat transfer occurs in the heater with internal energy generation, which can be characterized by

$$k_h \nabla^2 T + g = \rho_h c_h \frac{\partial T}{\partial t} \tag{2}$$

where k_h, c_h, and ρ_h are, respectively, thermal conductivity, specific heat, and density of the polyamide heater. The external heat source of polyamide heater is defines as g.

For scenarios where heaters are used on the rear surface (scenarios 2, 3 and 4), partial heat flux in the contour is considered. All other surfaces are exposed to the convection boundary condition with ambient air in the laboratory. Table 1 shows the thermophysical properties considered for each material composing the sample and used in the experiment.

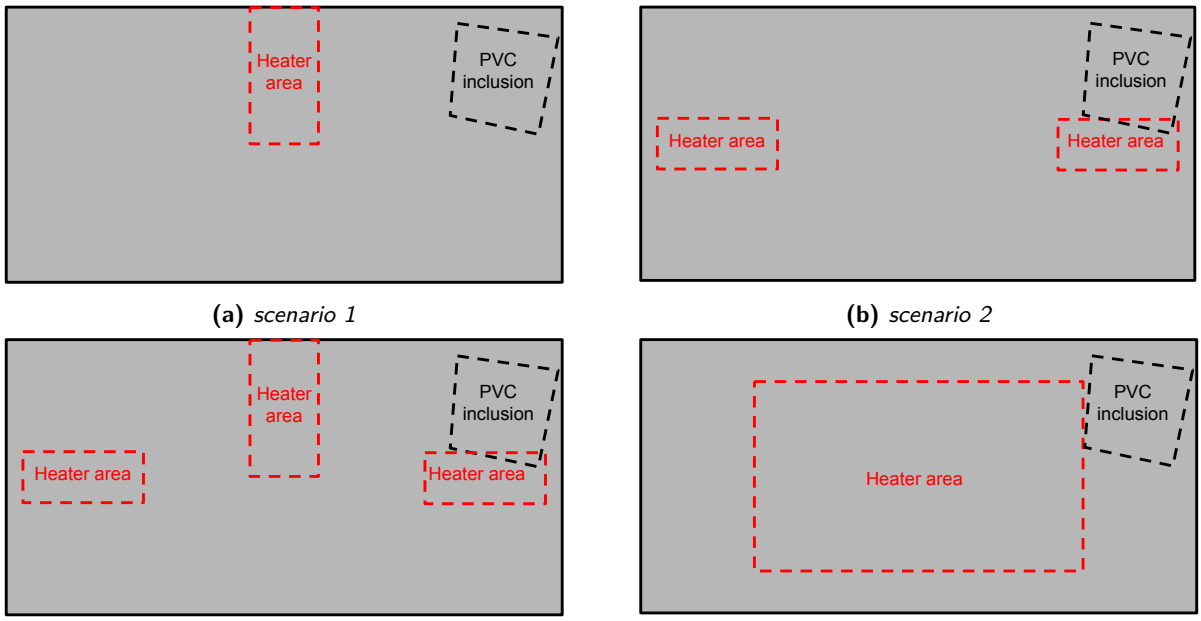

(a) *scenario 1* **(b)** *scenario 2*

(c) *scenario 3* **(d)** *scenario 4*

Fig. 3. *Four different scenarios for sample heating*

Table 1. *Thermophysical properties of the materials.*

Material	Thermal conductivity [W/(mK)]	Density [kg/m^3]	Specific heat [kJ/(kgK)]
ER-GF Composite	0.3376 [11]	2005	0.85
PVC-Inclusion	0.195 [12, 13]	1380 [14]	1.056 [14]
Polyimide-Heaters	0.29 [15]	1470 [15]	1.13 [15]

The values of density and specific heat for the epoxy resin - glass fiber composite were derived starting from [14, 16].

Numerical simulations were performed using the commercial software COMSOL® to solve the heat transfer problem using the same boundary conditions as the experiments. A mesh composed of 25479 tetrahedral elements was considered ideal after a mesh convergence study.

3. Results and Discussion

The first experiment refers to the use of scenario 1 where only a single heater was used to try to detect the defect using active thermography. A heating time of 360 s was used followed by 344 s of natural convection cooling at the laboratory ambient temperature of 297 K. The acquisition rate was 1 s, totaling 704 images acquired in the experiment. Figure 4a shows the thermographic image at the final stage of heating, where the central region can be seen with a maximum temperature of approximately 323 K due to the presence of the heater. No difference can be seen in the image between the region with the defect and the others. At all other times analyzed, it was also not possible to observe any difference in the thermal images that would characterize the presence of a defect in the sample. In fact the low thermal conductivity of the composite material (see Table 1) does not allow the heat to be easily diffused throughout the sample.

As the defect inserted in the sample proved to be difficult to detect for the chosen heating method, the normalized excess temperature is evaluated, i.e., the temperature at each point in the image was subtracted by the ambient temperature

(T_∞). Then the result is divided by the maximum existing excess temperature, as shown in Eq. 3.

$$\theta_n = \frac{T - T_\infty}{max(T - T_\infty)} \tag{3}$$

Figure 4b shows the thermographic image with just the normalized excess temperature from Fig. 4a, where it is observed that the maximum excess temperature is obtained in the heater region, which is why its value is equal to 1. The other points present values lower than 1, that is, characterizing lower temperature gains in relation to the heat source location. Even so, it was not possible to observe any region that characterizes the presence of the defect. For a better evaluation of the thermographic images, five lines were chosen in order to analyze in more detail what happened on the composite surface during the experiments, as shown in Fig. 4b. The lines intercepted the defect and non-defect region.

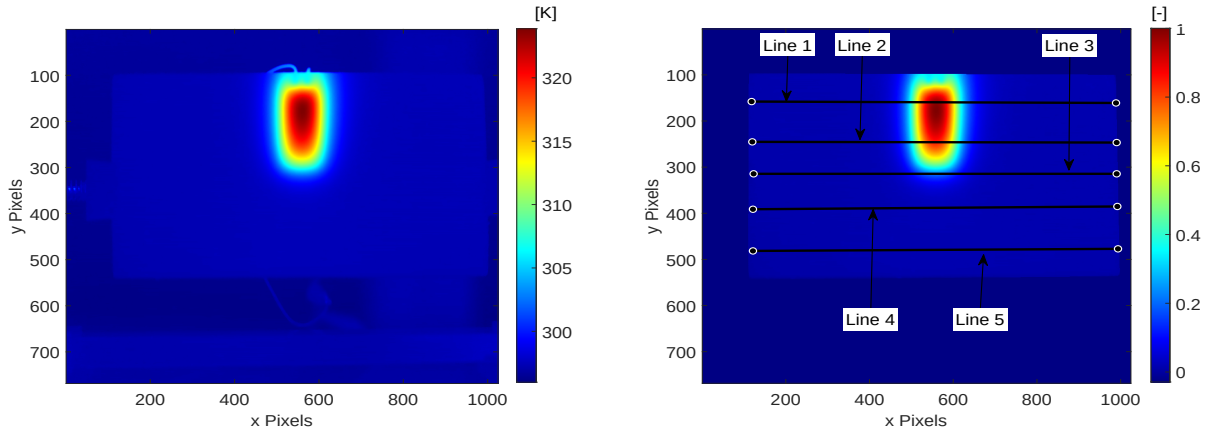

(a) *temperature distribution [K]* **(b)** *normalized excess temperature distribution [-]*

Fig. 4. *Thermographic images for scenario 1 at the end of heating*

Figure 5 shows the normalized temperature excesses for the lines in six instants of time 0, 120, 240, 360, 480, and 660 s. Each temperature line taken from the normalized thermographic image (as in the example in Fig. 4b) was divided by its respective maximum value. Thus, it is possible to observe that some region suspects that a defect may obtain a different heat gain. At instant 0 s, only the presence of noise can be observed, therefore, no additional discussion can be carried out, as shown in Fig. 5a. Figures 5b, 5c, and 5d show the instants of 120, 240, and 360 s during the heating period, respectively. At these times, the maximum temperature gain is observed in the central region due to the heater and no significant characterization of temperature change in the defect region. At cooling times of 480 and 660 s shown in Figs. 5e and 5f no thermal behavior that would help detect PVC inclusion was also observed. Therefore, scenario 1 was ineffective for detecting the defect, since the heat source was very far from the PVC inclusion and, therefore, the heating generated was not sufficient to thermally disturb the defect region in a different way than the healthy region.

Figure 6a shows a thermographic image obtained at the end of heating using the heating configuration of scenario 2, where it was still not possible to observe thermal changes that would characterize the defect. Figure 6b shows the normalized excess temperature and the five lines that will be analyzed, but also no defects were characterized in these images for all times.

Figure 7 shows the five normalized excess temperature lines for six different times. At the time of 60 s during heating, a non-symmetrical behavior in lines 2 and 3 can be observed, as shown in Fig. 7b. The right side of line 2 presents a lower temperature gain than the left side, this must have occurred because the PVC inclusion is close to the heated region, and therefore, the heat could not be transferred in the same way as in the region without defect due to the lower thermal conductivity of PVC compared to the composite. In line 4, the opposite is observed, that is, there was a greater temperature gain on the right side compared to the left. This occurred because the heat was more easily transferred downwards where the defect did not exist. Therefore, part of the amount of heat that was supposed to be transferred upwards (where the PVC was) went downwards, causing more heat to accumulate than on the left side. At times of 120, 180, and 240 s, the same trends were observed for lines 2 and 4, but with a smaller difference between the temperature gains, as shown in Figs. 7c, 7d, and 7e. At the time of 420 s shown in Fig. 7f, lines 1, 2, 3, and 4 show greater temperature gains on the right side. As this is the cooling phase, it can be said that heat loss is more efficient on the left side where there is no defect, which is why higher values were observed on the side where the PVC inclusion is located. Thus, scenario 2 was able to identify the presence of PVC inclusion due to the non-symmetrical thermal behaviors observed in the temperature gain lines.

Figures 8 and 9 show the results for the experiments using the scenario 3. Even with three heaters running at the same time in different locations, no imaging during heating and cooling was able to characterize the defect. The temperature

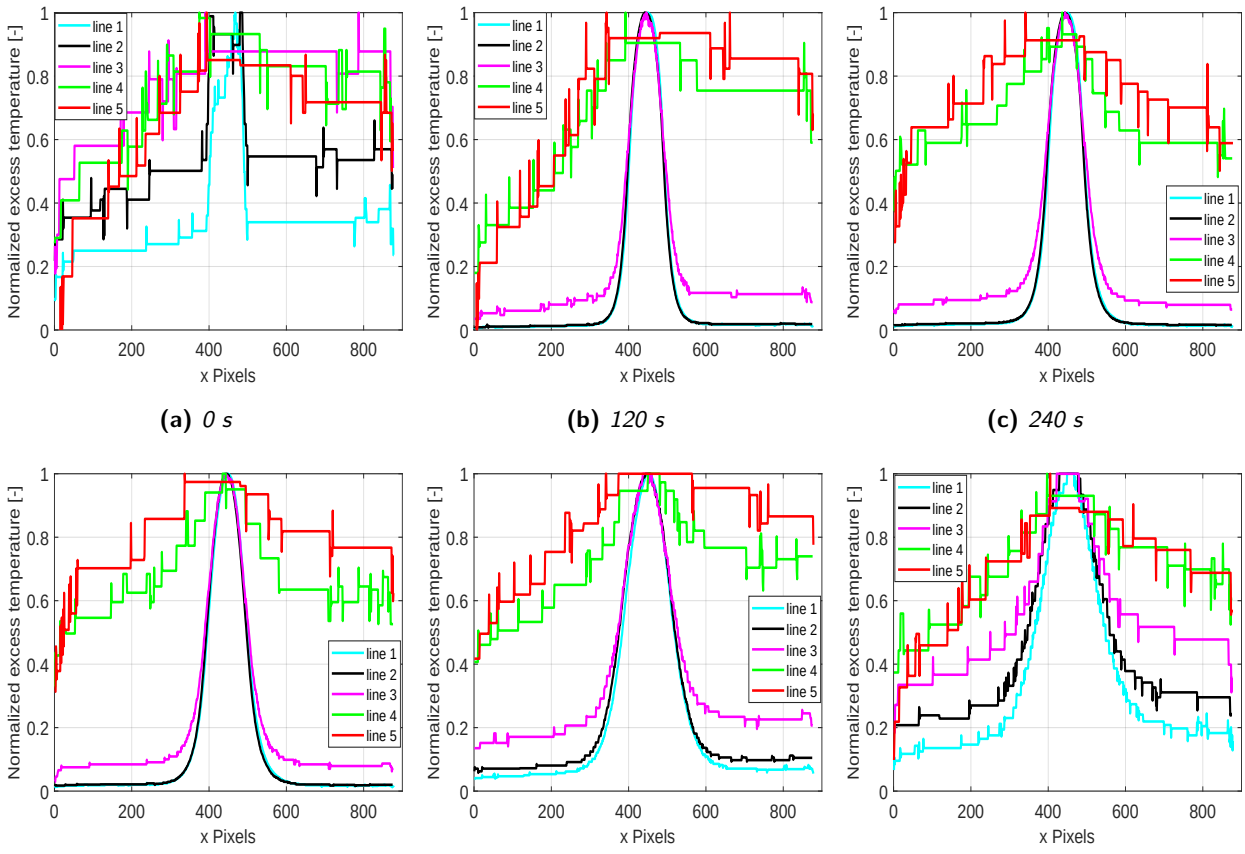

(a) *0 s* **(b)** *120 s* **(c)** *240 s*

(d) *360 s* **(e)** *480 s* **(f)** *660 s*

Fig. 5. *Normalized excess temperature lines for scenario 1.*

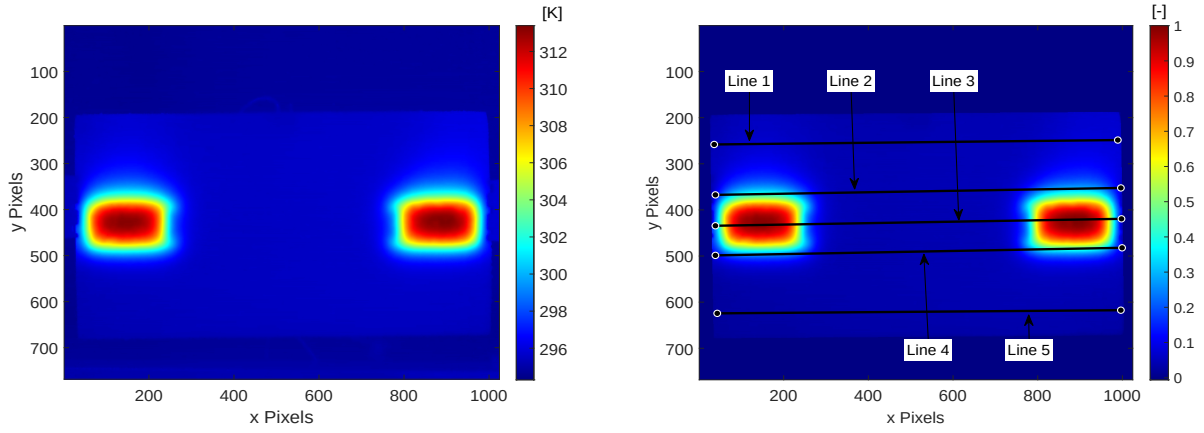

(a) *temperature distribution [K]* **(b)** *normalized excess temperature distribution [-]*

Fig. 6. *Thermographic images for scenario 2 at the end of heating*

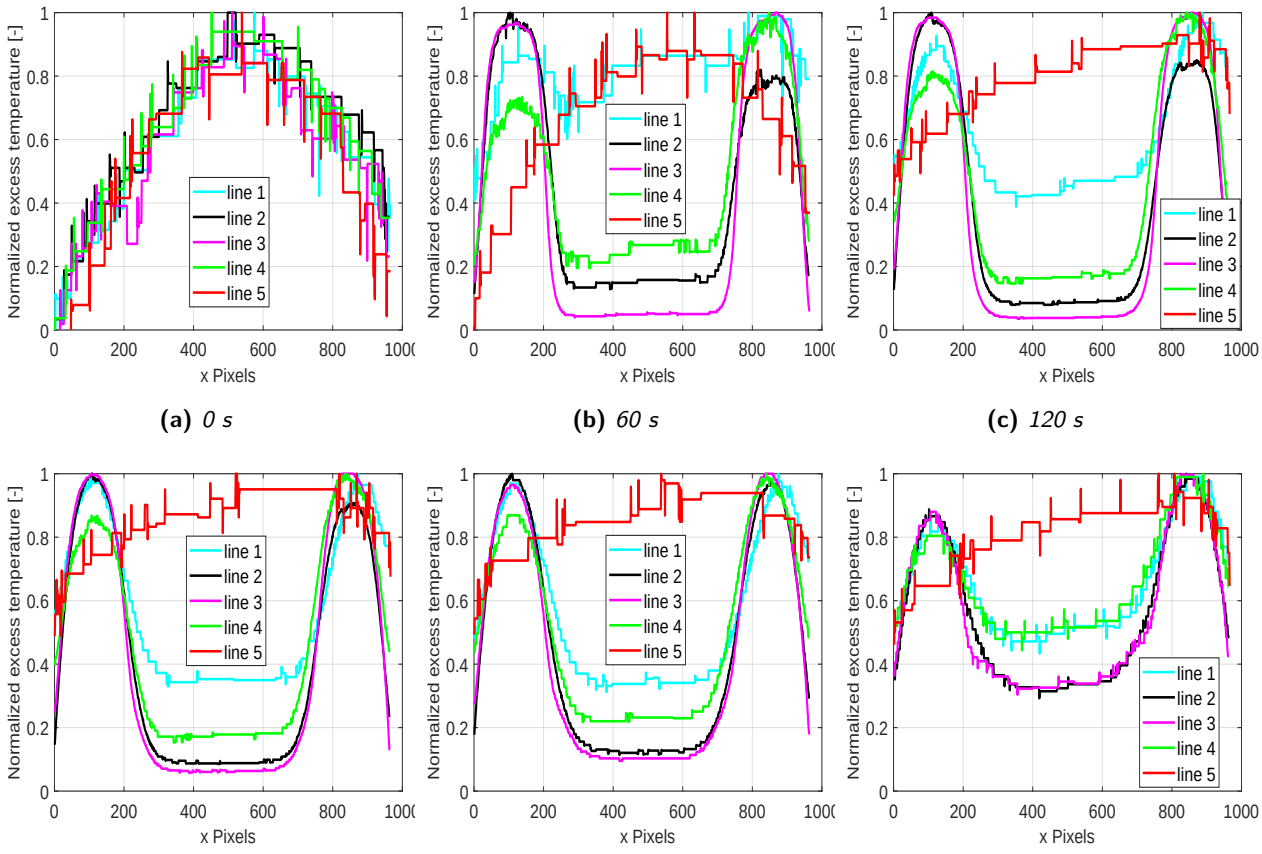

(a) *0 s* **(b)** *60 s* **(c)** *120 s*

(d) *180 s* **(e)** *240 s* **(f)** *420 s*

Fig. 7. *Normalized excess temperature lines for scenario 2.*

curves in Fig. 9 can show greater asymmetries for line 4 in relation to the scenario 2. Line 2 also shows asymmetries, especially during cooling. A greater temperature gain on the right side compared to the left side was also observed for line 1 at 420 s. Thus, scenario 3 was also able to present asymmetries in the temperature curves that can be interpreted until finding a possible defect in the composite. The advantage of this third configuration is having an additional heater, which can aid in the ability to find more defects due to increasing the chances of the heat source being closer.

In the configuration of the last scenario analyzed, Fig. 10a shows the thermography for the final heating time, where it can be seen that a region on the right side heated more than on the left side. This must have occurred because the inclusion of PVC made it difficult to transfer heat to the right side of the sample, resulting in the accumulation of heat in the region between the center of the composite and where the defect is located. Analyzing the excess temperature lines in Fig. 11, the 60 s instant shows a significant asymmetry between the two sides of the surface, especially in lines 1 and 2 that pass over the PVC inclusion. The right side presents an accumulation of heat due to the defect making heat transfer difficult. During the entire heating phase (120 s) and beginning of cooling (180 s) the same thermal behavior was observed. Therefore, scenario 4 was also able to present thermal asymmetries for a defective composite material.

In the numerical analysis, two configurations were analyzed considering the same parameters as experimental scenario 2. Figure 12a shows the transparent rear view with two heaters arranged in the same way as in the experiments - scenario 2a. Alternatively, in Fig. 12b, the heaters were placed to overlap the defect - scenario 2b.

Figure 13 shows the simulated thermal images at the final heating time of 120 s. Figure 13a shows the temperatures on the front surface of scenario 2a, where the image presents a thermal symmetry between the right and left side of the sample. When performing the subtraction between the right and left half of the thermal image, Fig. 13b shows the thermal contrast of this scenario, where it is possible to observe a small region of low temperature at the defect location and a region of high temperature below the defect. Figures 13c and 13d show the temperature distribution and thermal contrast for the simulation in scenario 2b. In this case, the reconstruction of the defect is of great interest, as the heat generated finds it more difficult to dissipate due to the presence of PVC, thus creating an image with low temperature contours that characterize the defect.

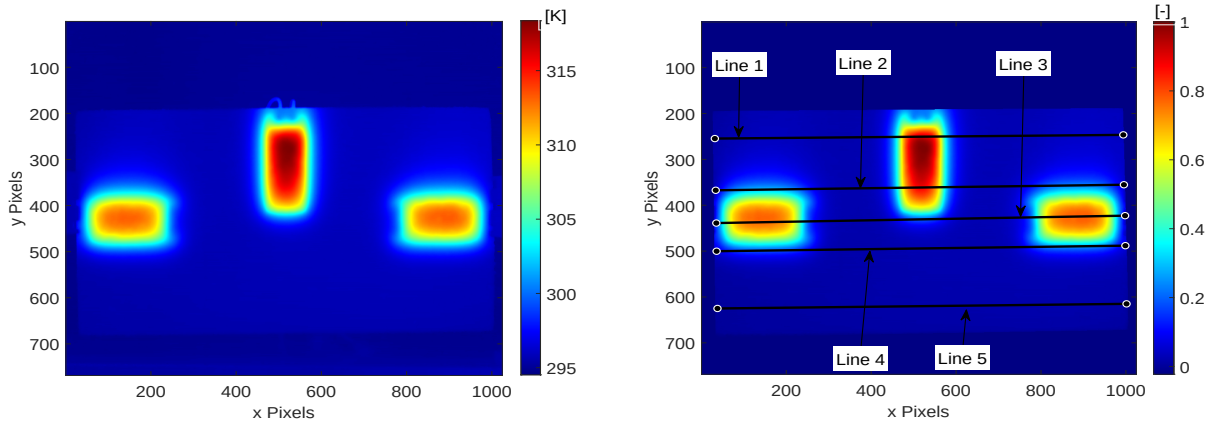

(a) *temperature distribution [K]* **(b)** *normalized excess temperature distribution [-]*

Fig. 8. *Thermographic images for scenario 3 at the end of heating*

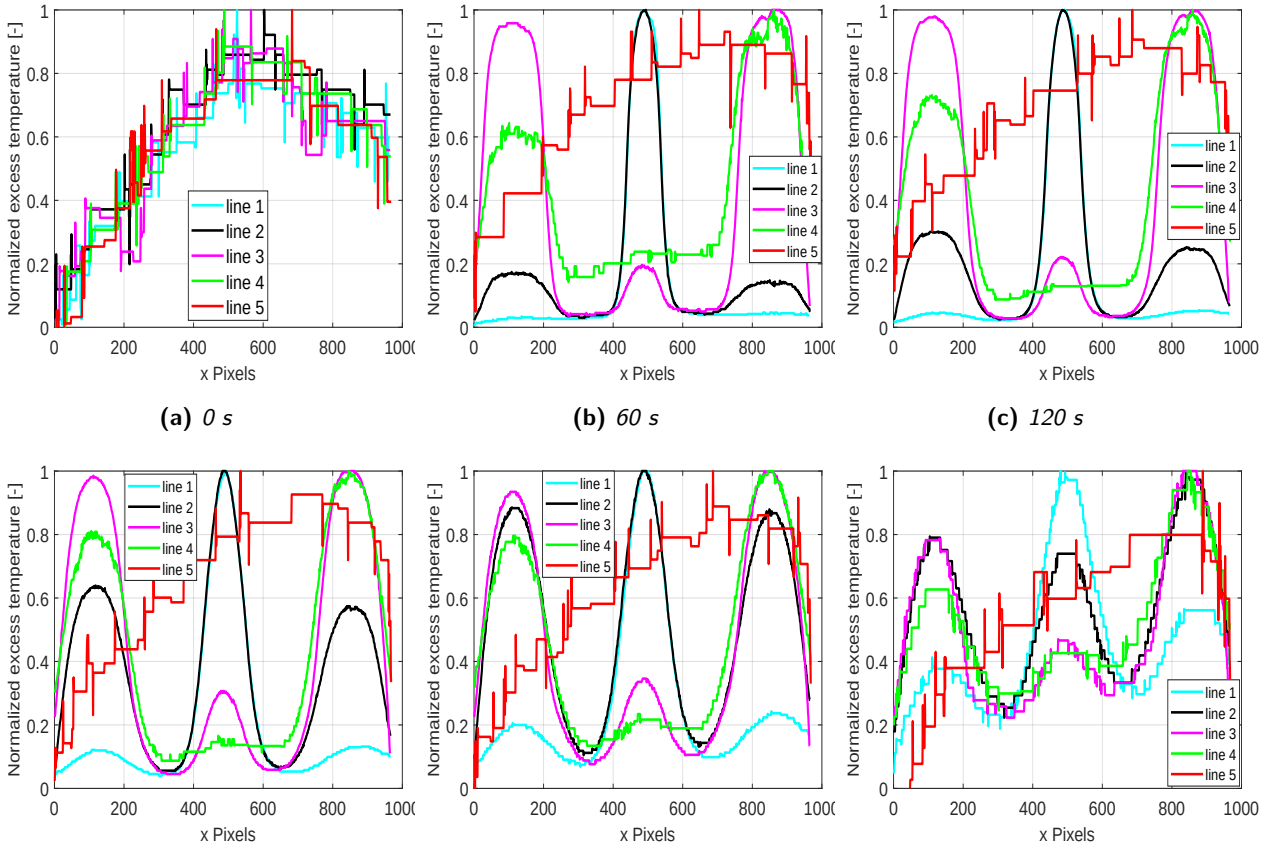

(a) *0 s* **(b)** *60 s* **(c)** *120 s*

(d) *180 s* **(e)** *240 s* **(f)** *420 s*

Fig. 9. *Normalized excess temperature lines for scenario 3.*

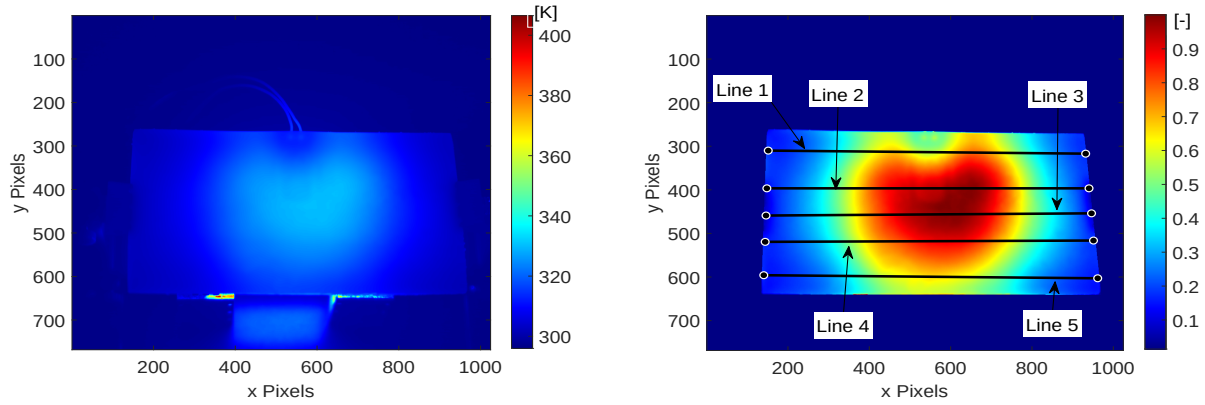

(a) *temperature distribution [K]* **(b)** *normalized excess temperature distribution [-]*

Fig. 10. *Thermographic images for scenario 4 at the end of heating*

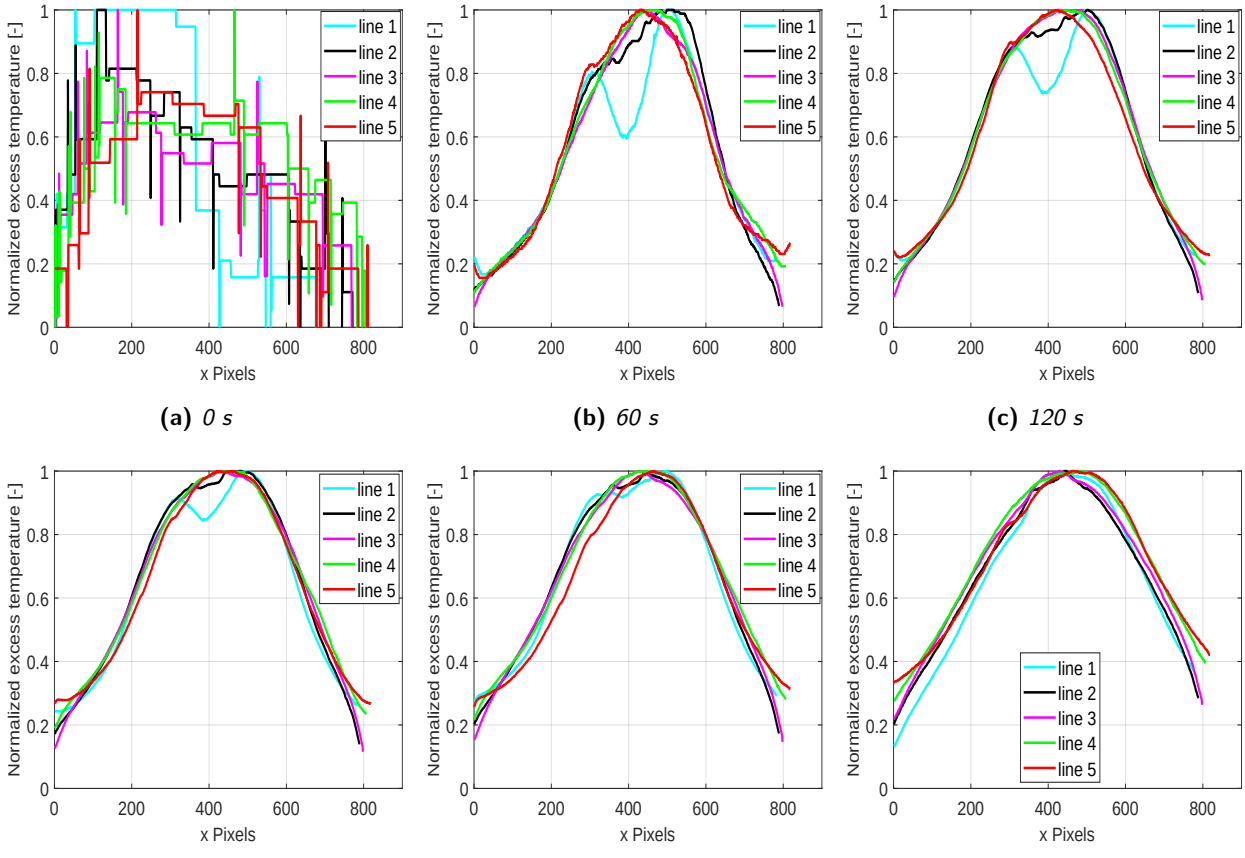

(a) *0 s* **(b)** *60 s* **(c)** *120 s*

(d) *180 s* **(e)** *240 s* **(f)** *420 s*

Fig. 11. *Normalized excess temperature lines for scenario 4.*

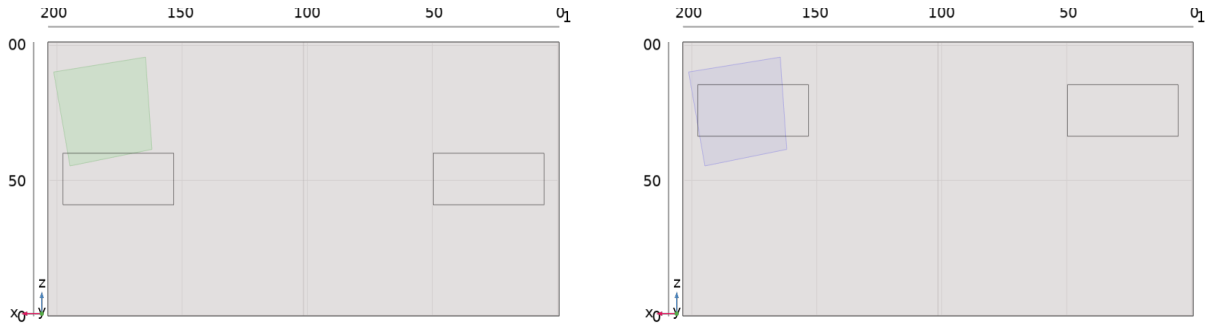

(a) *Scenario 2a* **(b)** *Scenario 2b*

Fig. 12. *Transparent back view of numerical model*

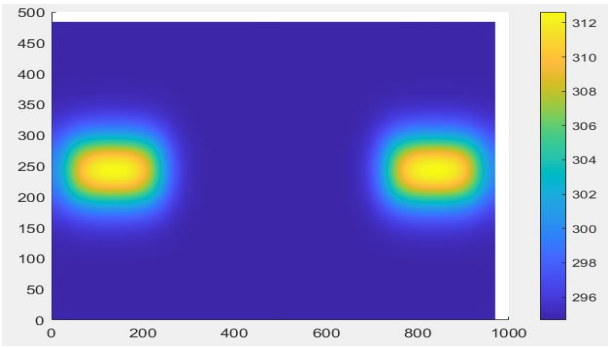

(a) *Scenario 2a - temperature*

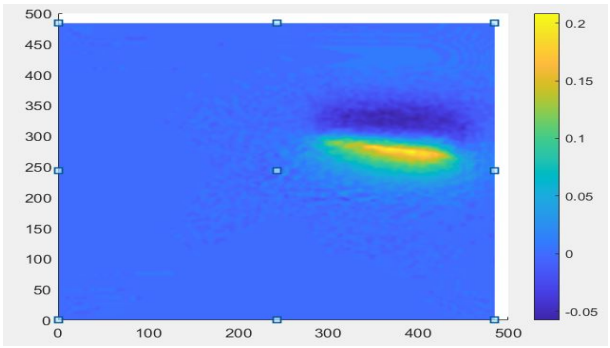

(b) *Scenario 2a - thermal contrast*

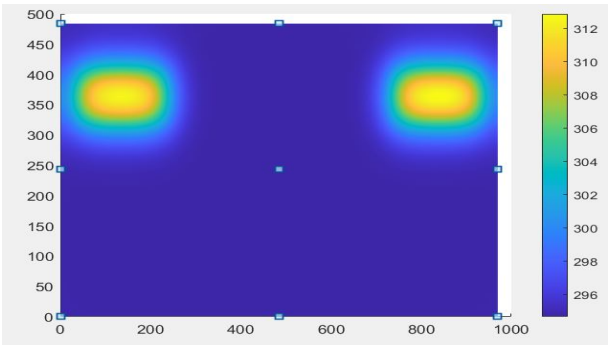

(c) *Scenario 2b - temperature*

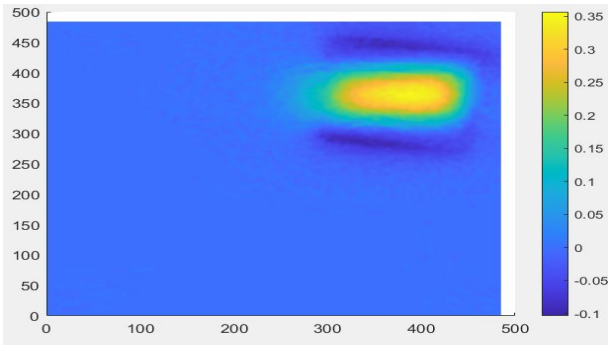

(d) *Scenario 2b - thermal contrast*

Fig. 13. *Numerical thermal images at 120 s [K]*

4. Conclusion

In this active thermography experimental study, four different scenarios were evaluated to identify a defect in composite material structures of turbine blades. The results obtained provided a comprehensive view of the capabilities and limitations of each experimental setup. Scenario 1 did not show sensitivity for detecting the defect due to the significant distance between the heat source and the PVC inclusion. As the composite material has low thermal conductivity, the heating method chosen in this work requires the heat source to be close to the defect to be able to help detect the problem.

Scenario 2 with two heaters was able to present asymmetries between the sides with and without defects, making it possible to use the method to track this type of failure. Scenario 3 also presented thermal responses capable of verifying the presence of problems in the composite material. Scenario 4, which used a larger heater in the central region, proved to be effective in characterizing the defect and may be more appropriate for a greater variety of anomaly possibilities due to its

greater capacity to heat the composite, also increasing the possibility of reducing the distance between the heat source and the defect. Numerical analysis showed that if the heater and inclusion are overlapping, the defect reconstruction can be considered of great interest.

Based on the analyses carried out, it is possible to conclude that the appropriate heating depends on the specific characteristics of the sample and the type of defect to be identified. The heating applied needs to guarantee that the heat will be able to reach the still unknown defect, therefore, multiple heaters or a large heater may be the best strategy. The work, explained in a didactic way, should be considered of interest for university students passionate of infrared thermography. The work, indeed, leaves open the doors for more accurate quantitative evaluations of the results already found.

5. Acknowledgments

The authors would like to thank Prof. Francesco de Paulis (University of L'Aquila, Italy) for the fundamental help provided in building the experimental setup.

References

[1] Hadi Sanati, David Wood, and Qiao Sun. Condition monitoring of wind turbine blades using active and passive thermography. *Applied Sciences*, 8(10):2004, 2018.

[2] Zhuoqiao Wu, Ning Tao, Cunlin Zhang, and Jian-gang Sun. Prediction of defect depth in gfrp composite by square-heating thermography. *Infrared Physics & Technology*, 130:104627, 2023.

[3] AP PONTELLO. Thermography for nondestructive testing of fuel filtration equipment and other applications. In *MATERIALS EVALUATION*, volume 30, page A35. AMER SOC NON-DESTRUCTIVE TEST 1711 ARLINGATE LANE PO BOX 28518, COLUMBUS, OH ..., 1972.

[4] C Galleguillos, A Zorrilla, A Jimenez, L Diaz, ÁL Montiano, M Barroso, A Viguria, and F Lasagni. Thermographic non-destructive inspection of wind turbine blades using unmanned aerial systems. *Plastics, Rubber and Composites*, 44(3):98–103, 2015.

[5] Tamara Worzewski, Rainer Krankenhagen, Manoucher Doroshtnasir, Mathias Röllig, Christiane Maierhofer, and Henrik Steinfurth. Thermographic inspection of a wind turbine rotor blade segment utilizing natural conditions as excitation source, part i: Solar excitation for detecting deep structures in gfrp. *Infrared physics & technology*, 76:756–766, 2016.

[6] Darryl P Almond, Stefano L Angioni, and Simon G Pickering. Long pulse excitation thermographic non-destructive evaluation. *NDT & E International*, 87:7–14, 2017.

[7] Friederike Jensen, Josefa Feline Jerg, Michael Sorg, and Andreas Fischer. Active thermography for the interpretation and detection of rain erosion damage evolution on gfrp airfoils. *NDT & E International*, 135:102778, 2023.

[8] Stefano Sfarra, Antonio Cicone, Bardia Yousefi, Stefano Perilli, Leonardo Robol, and Xavier PV Maldague. Maximizing the detection of thermal imprints in civil engineering composites via numerical and thermographic results pre-processed by a groundbreaking mathematical approach. *International Journal of Thermal Sciences*, 177:107553, 2022.

[9] Giampaolo D'Alessandro and Filippo de Monte. On the optimum experiment and heating times when estimating thermal properties through the plane source method. *Heat Transfer Engineering*, 43(3-5):257–269, 2021.

[10] Giampaolo D'Alessandro, Filippo de Monte, Suelen Gasparin, and Julien Berger. Comparison of uniform and piecewise-uniform heatings when estimating thermal properties of high-conductivity materials. *International Journal of Heat and Mass Transfer*, 202:123666, 2023.

[11] MJ Assael, KD Antoniadis, and D Tzetzis. The use of the transient hot-wire technique for measurement of the thermal conductivity of an epoxy-resin reinforced with glass fibres and/or carbon multi-walled nanotubes. *Composites science and technology*, 68(15-16):3178–3183, 2008.

[12] Vishal Mathur, Pramod Kumar Arya, and Kananbala Sharma. Estimation of activation energy of phase transition of pvc through thermal conductivity and viscosity analysis. *Materials Today: Proceedings*, 38:1237–1240, 2021.

[13] Gil De Carvalho, Elisabete Frollini, and Wilson Nunes Dos Santos. Thermal conductivity of polymers by hot-wire method. *Journal of applied polymer science*, 62(13):2281–2285, 1996.

[14] Chemical Retrieval on the Web. Polymer database. Accessed: October 2022.

[15] Ube corporation. Accessed: October 2022.

[16] Final materials. Accessed: October 2022.